

Giant enhancement and quick stabilization of capacitance in antiferroelectrics by phase transition engineering

Received: 2 August 2024

Accepted: 19 October 2024

Published online: 28 October 2024

Check for updates

Tengfei Hu^{1,2}, Zhengqian Fu¹✉, Xiaowei Liu¹, Linhai Li¹, Chenhong Xu¹, YongXin Zhou¹, Fei Cao¹, Jiakexia¹, Xuefeng Chen¹✉, Genshui Wang^{1,2}✉ & Fangfang Xu^{1,3}✉

The antiferroelectric-ferroelectric phase transition is a basic principle that holds promise for antiferroelectric ceramics in high capacitance density nonlinear capacitors. So far, the property optimization based on antiferroelectric-ferroelectric transition is solely undertaken by chemical composition tailoring. Alternately, here we propose a phase transition engineering tactic by applying pulsed electric stimulus near the critical electric field, which finally results in -54.3% enhancement and quick stabilization of capacitance density in $\text{Pb}_{0.97}\text{La}_{0.02}(\text{Zr}_{0.35}\text{Sn}_{0.55}\text{Ti}_{0.10})\text{O}_3$ antiferroelectric ceramics. Ex-situ and in-situ structural characterizations show that electric stimuli can induce the charming successive structural evolution, including domain evolution from multidomain to monodomain state, and modulation period change from 7.49 to 7.73. Structure-property correlation indicates that the antiferroelectric-ferroelectric phase transition engineering mainly stems from the unexpected irreversible recovery of the modulated structures. The present findings would deepen the understanding of the structural phase transition and provoke composition-independent post-treatment property innovation in the incommensurate antiferroelectric materials and devices.

Multilayer ceramic capacitors (MLCCs) have excellent dielectric performance and are widely used in modern electronic devices¹⁻⁷. High capacitance density is extremely desired for MLCCs to meet their increasing demand in the electronics market⁸, e.g. filter capacitors. Benefitting from the positive voltage coefficient, antiferroelectric (AFE) ceramics become one of the most promising candidates for high capacitance density nonlinear capacitors⁹⁻¹¹.

The realization of energy storage and release of AFE capacitors is based on the reversible phase transition between antiferroelectric state and ferroelectric (FE) state^{12,13}. Generally, phase transition engineering has been an effective way to tailor the physical properties and functionalities of materials¹⁴⁻¹⁸. For instance, Si_3N_4 ceramics can

generate -20% room temperature plasticity deformation by controlling stress-induced phase transition with successive bond switching at the coherent interfaces¹⁴, and NiCoFeGa alloy can achieve unprecedented superelasticity with no hysteresis by introducing continuous martensitic transition¹⁵.

Similarly, the performance of AFE capacitors has been proved to be able to be optimized by controlling the AFE-FE phase transition^{19,20}. However, so far, optimization of electrical performance has been solely undertaken by chemical substitution or doping²¹⁻³⁰. For example, numerous chemical elements (A sites: La^{3+} , Ca^{2+} , Sr^{2+} , etc.; B-sites: Sn^{4+} , Ti^{4+} , Nb^{5+} , etc.) have been incorporated in PbZrO_3 with different ratios for adjusting the switching field and thus optimizing the

¹State Key Laboratory of High Performance Ceramics and Superfine Microstructures & The Key Lab of Inorganic Functional Materials and Devices, Shanghai Institute of Ceramics, Chinese Academy of Sciences, Shanghai 200050, China. ²School of Chemistry and Material Science, Hangzhou Institute for Advanced Study, University of Chinese Academy of Sciences, 1 Sub-lane Xiangshan, Hangzhou 310024, China. ³School of Physical Science and Technology, ShanghaiTech University, Shanghai 201210, China. ✉e-mail: fmail600@mail.sic.ac.cn; xfchen@mail.sic.ac.cn; genshuiwang@mail.sic.ac.cn; ffxu@mail.sic.ac.cn

dielectric properties^{21–30}. Recently, several in-situ experiments using X-ray diffraction or neutron diffraction show that the electric field can modify the domain configurations^{31,32}, e.g. triggering reorientation of domain structures. Therefore, it is natural to wonder whether the behaviors of AFE-FE phase transition can be adjusted by electric field for optimizing the performance of AFE capacitors.

Here we report that they can be. After utilizing the pulsed electric stimulus near the critical electric field to perform AFE-FE phase transition engineering, we achieved ~54.3% capacitance enhancement and quick stabilization in the AFE ceramics. Ex-situ and in-situ experiments are designed to characterize the structural evolution during the electric stimuli, which then shows the role of the incommensurate modulated structures in the phase transition engineering. These results indicate that the AFE-FE phase transition engineering could be a simple post-treatment route for tailoring the performance of AFE materials, which is more applicable for incommensurate AFEs.

Results

AFE-FE phase transition engineering via pulsed electric stimulus

The concept of AFE-FE phase transition engineering on the $\text{Pb}_{0.97}\text{La}_{0.02}(\text{Zr}_{0.35}\text{Sn}_{0.55}\text{Ti}_{0.10})\text{O}_3$ (hereafter denoted as PLZST) ceramics is illustrated in Fig. 1. Generally, the electric-field-induced AFE-FE transition can manifest itself as characteristic double hysteresis loops during polarization-electric field measurement (Fig. 1a). It can be seen that the AFE-FE phase transition occurs at a narrow electric field range close to the forward transition electric field (E_{AF}), where the AFE and FE states show strong competition^{22,33}. This character implies that it is

possible to change the AFE state and the corresponding properties if we apply a pulsed electric stimulus at E_{AF} . We called this process as phase transition engineering as illustrated in Fig. 1b. For demonstrating the AFE-FE phase transition engineering on PLZST, the change of capacitance with different processing parameters including electric field intensity, time and temperature, are studied meticulously (see Figure S1). It is then found that the direct current (DC) electric field at E_{AF} and the processing time close to 1 s are enough to achieve the giant capacitance enhancement and quick stabilization at any temperature below the Curie temperature.

Then, we measured the room-temperature capacitance densities of PLZST ceramics after phase transition engineering under different electric fields. As seen in Fig. 1c, the evolution of capacitance density displays two characteristics. Firstly, on each curve for numbers of pulsed stimuli at a certain electric field, the capacitance density abruptly ascends under the first stimulus, then keeps slightly increasing in subsequent dozens of stimuli and finally saturates at a certain value. Among these stimuli processes, capacitance enables faster stabilization when the electric fields just exceed the E_{AF} (e.g., 10 times stimuli @ 8.2 kV/cm vs 30 times stimuli @ 7.0 kV/cm). Secondly, the capacitance density keeps increasing with increase of electric field for stimuli, where the increment of the capacitance density becomes slowing down when approaching to high electric fields close to E_{AF} and finally reaches a maximum value. The polarization-electric field hysteresis loops (Figure S2) and X-ray diffraction patterns (Figure S3) shows the minor change in energy-storage performance and no significant difference in crystal structure after pulsed electric stimuli.

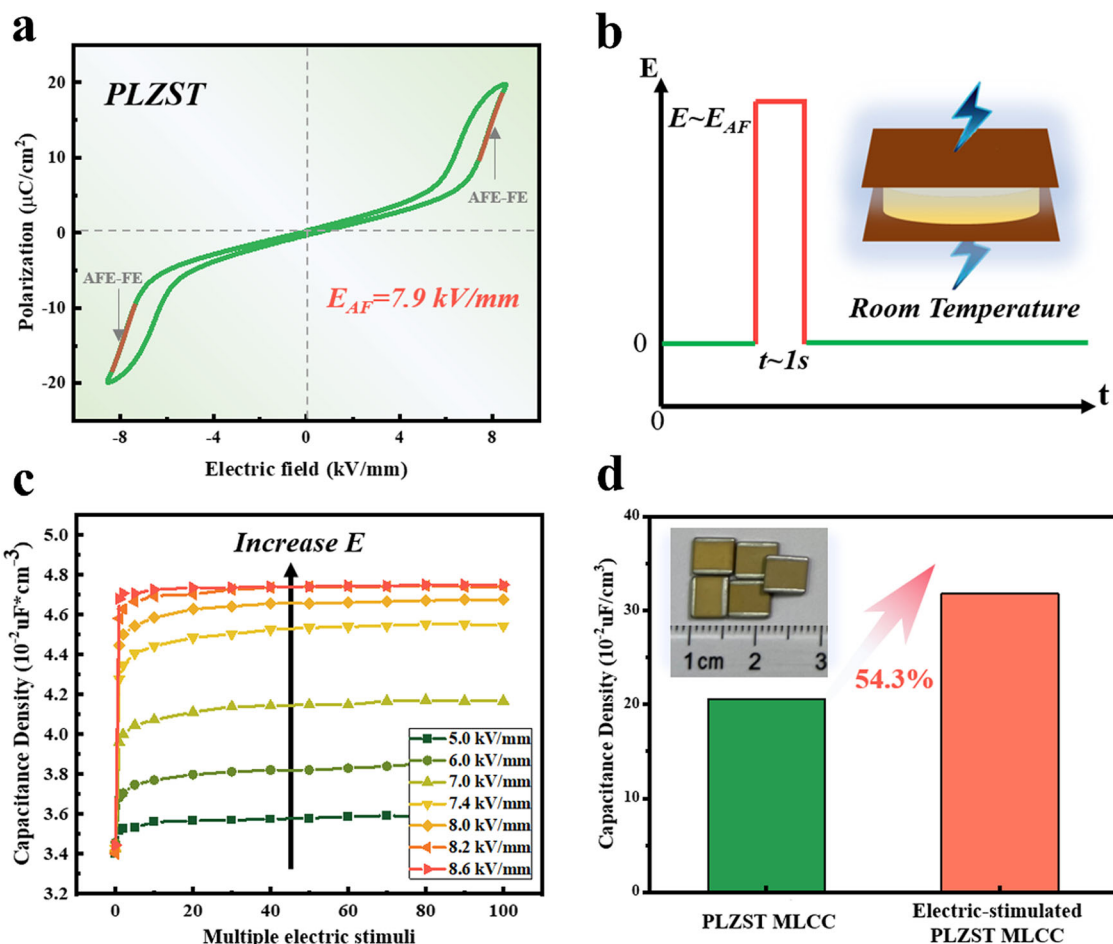


Fig. 1 | The concept and demonstration of AFE-FE phase transition engineering on PLZST capacitor. a Polarization-electric field hysteresis loop. **b** Schematic of the optimized pulsed electric-stimulated processing. **c** Evolution of ceramic capacitance

density after multiple pulsed electric stimuli under different electric fields. **d** Comparison of multilayer capacitance density between the fresh sample and that after a single electric stimulus. The insert is the optical photo of the PLZST MLCCs.

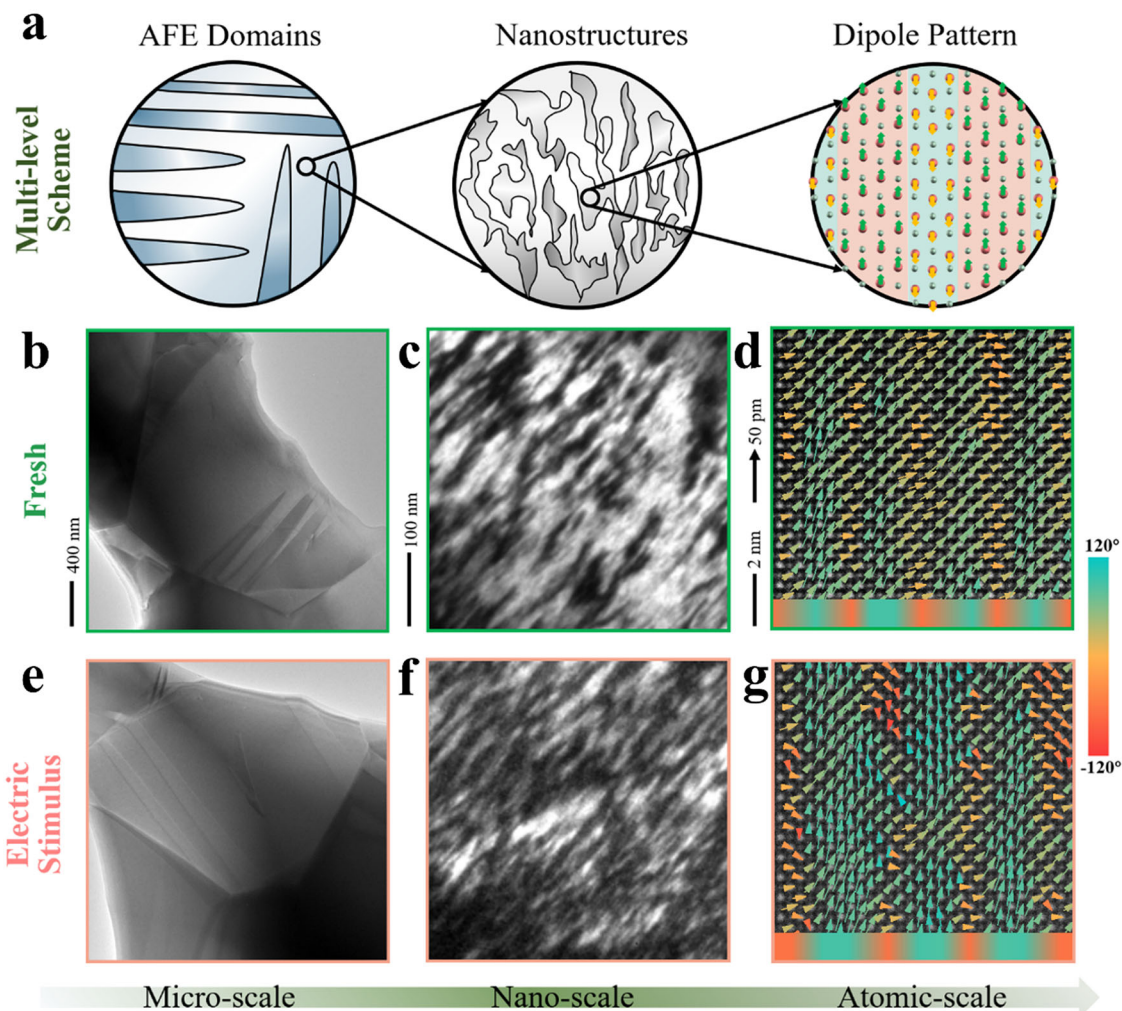


Fig. 2 | Contrastive analysis of fresh and single electric-stimulated PLZST at different scales. **a** Schematic diagram of cross-scale structures in AFE ceramics. **b, e** AFE domain structures, **(c, f)** dark-field images using a satellite spot and **(d, g)**

atomic displacement mappings based on STEM-HAADF images of fresh and single electric-stimulated (the applied electric field is near E_{AF}) samples, respectively. The horizontal direction to the right is $[110]$ direction in **(d, g)**.

Overall, by applying AFE-FE phase transition engineering on PLZST, it can bring about obvious capacitance enhancement of -39.6% and realize quick stabilization of the subsequent performances, which is critical for the practical applications. We then prepared the multi-layer ceramic capacitors (MLCCs, 23 layers) via inter-stacking the -13.5 μm thick PLZST layers and -2.0 μm thick Ag-Pd layers (Fig. 1d; Figure S4), and deal with them by AFE-FE phase transition engineering. Finally, a maximum capacitance enhancement of -54.3% was achieved in MLCCs (Fig. 1d).

Ex-situ microstructural analysis of phase transition engineering

To get insight into the underlying mechanism of AFE-FE phase transition engineering, we conducted the ex-situ microstructural analysis of the fresh and single electric-stimulated PLZST samples, as shown in Fig. 2. According to our previous studies^{34–36}, PbZrO_3 -based AFE materials always exhibit hierarchical microstructures, *i.e.*, Pb cations spontaneously occur displacive modulation at atomic-scale, but the modulated supercell cannot form a perfect long-range arrangement while always displays textured interfacial defects and nanostructures for lowering the system energy. These nanostructures with different orientations finally compose of the AFE domains at micron scale.

After single electric stimulus, it can be seen that AFE domains do not change significantly in morphology (Fig. 2b, e; Figure. S5). But of particular interest is that the electric-stimulated PLZST sample exhibits

higher density of interfacial defects (Fig. 2c, f) and wider Pb-cations displacive segments than the fresh sample (Fig. 2d, g), where the nearly parallel short interface fragments on an identical $\{110\}$ plane frequently shift to form multiple steps due to local changes of modulation period, thus leading to the appearance of more random or curved shapes of the interfacial defects at lower magnification. Thus, the electric stimulus has induced increasing of the modulation period, which is also confirmed by statistical analysis on the selected-area electron diffraction pattern, in which the modulation period can be determined by measuring the distance of satellite spot to the main reflection (see Figure S6a, 6b). By examining more than 28 different area (Figure S6c), the average modulation period is obtained to be 8.10 ± 0.27 and 7.46 ± 0.12 in the electric-stimulated and fresh sample, respectively. The changed modulation structures under zero field means the changed polarization switching process under electric field (see Figure. S7). These observations indicate that the so-called reversible AFE-FE phase transition in double hysteresis loop is not rigidly reversible in actual.

In-situ microstructural analysis of phase transition engineering

Based on the above observations, we then carried out in-situ biasing TEM experiments using two different modes of electric field loading, which were designed for further understanding the capacitance enhancement and stabilization, respectively. One of modes was that the electric fields gradually increased during the numbers of stimuli till

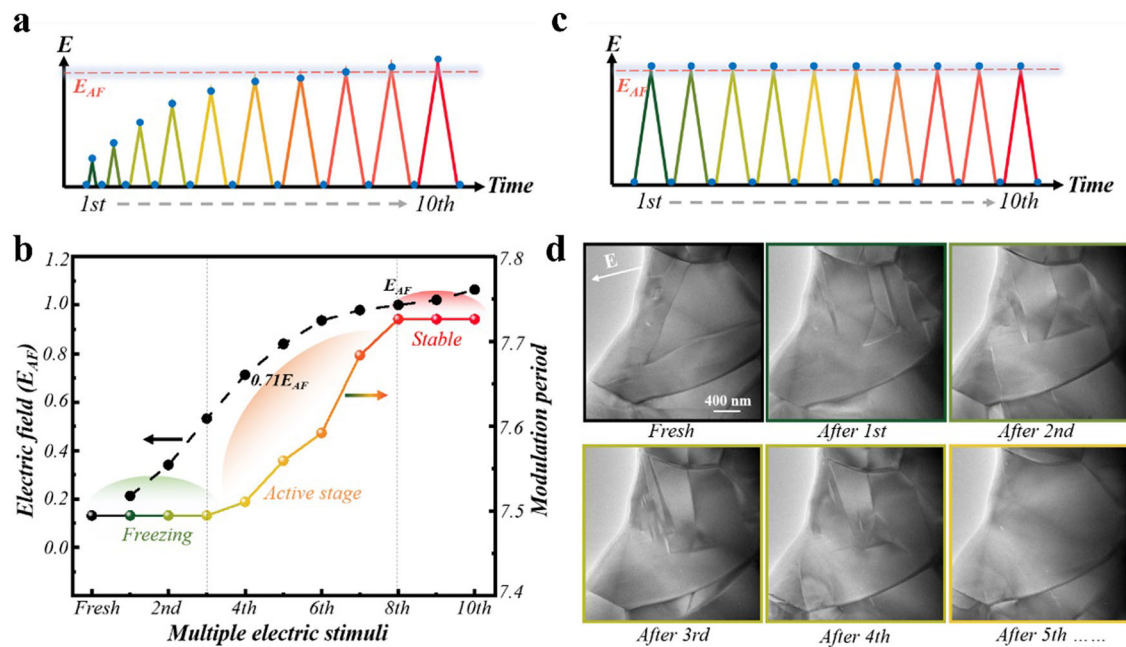


Fig. 3 | Phase transition behaviors. **a, c** The diagrams of two modes of electric field loading in TEM, i.e. **(a)** stimuli with gradual increase of electric field until exceeding E_{AF} and **(c)** numbers of stimuli at the same electric field just above E_{AF} . The blue dots represent the loading electric fields during each process. **b** Changes of modulation period after each electric stimulus as function of electric field in **(a)** mode, showing

three stages with increasing electric fields, namely freezing stage, active stage and stable stage. The black and colorful spots represent the loading electric field during each electric stimulus and the modulation period after each stimulus, respectively. **d** Domain evolution after multiple electric stimuli at the same electric field above E_{AF} in **(c)** mode. The white arrow points to the direction of electric field loading.

that exceeding E_{AF} (Fig. 3a), and the other mode was that a fixed electric field was applied just beyond E_{AF} during the successive ten times of stimuli (Fig. 3c).

For the first electric-stimuli mode (Fig. 3a), Fig. 3b shows the evolution of modulation period after each electric stimulus as function of electric field. Interestingly, the increase of modulation period can be divided into three different stages with stimuli sequence (Fig. 3b; Fig. S8), i.e., the modulation period remains unchanged (namely freezing stage) when the electric field is far below E_{AF} ; the modulation period wakes up and continuously increases (7.49–7.73) under stimuli at higher electric field ($0.71E_{AF}$ – $1.0E_{AF}$, namely active stage); and the modulation period reaches the maximum value and keeps still (namely stable stage) after the electric fields exceed the E_{AF} . The occurrence of phase transition from AFE to FE phase can be easily evidenced by the disappearance of both AFE domains and satellite spots (Fig. S9). It can be found that the evolution of modulation period coincides with the capacitance enhancement in Fig. 1c, i.e., the modulation period and the capacitance density increase synchronously with increase of stimulating electric field and then both tend to be stable when the electric fields exceed E_{AF} .

For the second electric-stimuli mode (Fig. 3c), i.e. ten stimuli at the identical electric field just above E_{AF} , it is found that the AFE domain structures keep changing during the first four stimuli (Fig. 3d; Fig. S10), in which the number of domain walls increases and the orientation of majority of domain walls tends to be either parallel or perpendicular to the direction of loaded electric field. From the 5th stimulus, the domain walls immediately become invisible, i.e. the grain exhibits the monodomain state. Similarly, the modulation period (Fig. S11) shows the well corresponded changes with domain evolution as well as the capacitance change (see each curve in Fig. 1c). That is, the modulation period shows the first rapid improvement and then gradually stable trend.

Structure-property correlation underlying the phase transition engineering

It is generally believed that the centrosymmetric shape of the double hysteresis loops suggests complete reversibility of the AFE-FE phase

transition, otherwise a typical FE hysteresis loop would be observed (see Fig. S12)^{37–39}. However, our present work indicates that the AFE-FE transition underlying the double hysteresis loops is actually the irreversible structural transformation in PLZST, where the most notable character is that the modulation period cannot recover. As illustrated in Fig. 4a, the applied electric field drives the antiparallel dipole modulation to change to the parallel dipole ordering, and then back to the antiparallel dipole modulation but with a larger modulation period. When the applied electric field keeps at E_{AF} , dynamic equilibrium between AFE and FE state could still be reserved (Fig. S13), which provides the strong basis for phase transition engineering.

Because the modulation period is a manifestation of the supercell size for dipole arrangement, the larger modulation period refers to the decrease of interactions between the nearest neighboring dipoles with opposite directions, which will lead to the increased dielectric constant and thus the enhanced capacitance density^{34,40}. The close correlation between modulation period and capacitance density has been explicitly illustrated in the present electrical measurements (Fig. 1c) and structural characterization (Fig. 3b, d). If the electric field stimulus ($E_{stimulus}$) is much small than the starting field of AFE-FE transition (e.g., $0.4E_{AF}$, as shown in the freezing stage), it cannot trigger the AFE-FE transition at all and thus both modulation period and capacitance density are frozen. Once the $E_{stimulus}$ keeps on increasing till close to the E_{AF} (active stage) as schemed in Fig. 4b, the recovered AFE state exhibits an increased modulation period with denser interface (Fig. 2c, f) and thus achieves the continuous enhancement of capacitance density.

Further increasing the electric field of stimulus over E_{AF} does not seem to make any difference for the enhancement of capacitance density. Thus, the E_{AF} is high enough for obtaining the maximum increment of modulation period. The stable stage under larger electric field stimuli (see the corner region in Fig. 4b) is mainly contributed from the inner structural stability, especially the evolution of multidomain to monodomain state according to the observation in Fig. 3d. However, it is worth noting in Fig. 4b and

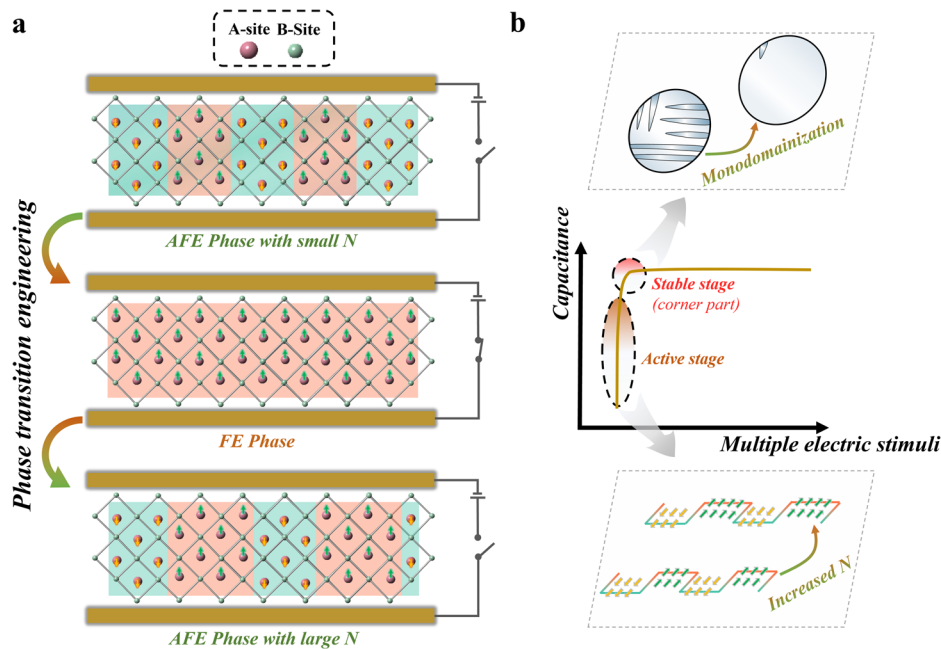


Fig. 4 | The underlying mechanism of phase transition engineering. **a** The model of phase transition engineering with electric-field-induced polarization switching. The N stands for the modulation period. **b** Diagram of one-to-one

structure–property correlation, showing the evolution of the multilevel structures at different stages of the electric field stimuli.

Fig. 1c that as soon as the curve turns at the corner, approximately no further increase of capacitance density takes place. That is, the change of modulation period after the first few electric field stimuli has provided a solid basis for the stabilization of capacitance. This phenomenon implies that the modulated structure rather than the domain structure in AFE materials should be the dominant factor governing the macroscopic properties, which is very different from the strong coupling of intrinsic and extrinsic contribution in piezoelectrics^{41,42}. In addition, the observed irreversible recovery is not universal for all AFE materials (see Fig. S14), but may only be applicable for the incommensurate ones. It seems that the thermodynamic equilibrium obtained during high-temperature sintering could be broken down by a dynamic process with an external electric field loading at room temperature, during which the strength of high-energy anti-dipole interaction is attenuated through increasing the modulation period, thus illustrating an irreversible phase transition. Finally, a new dynamic equilibrium is achieved and enables giant enhancement and quick stabilization of capacitance.

Discussion

In summary, we have achieved a 54.3% enhancement and subsequent stable performance of capacitance density in PLZST AFE capacitors by AFE-FE phase transition engineering. This strategy can maximize the effect only via applying pulsed electric stimuli at the critical field for the AFE-FE phase transition. It is found that the mechanism of phase transition engineering mainly derives from the irreversible recovery of modulated structures. In practical applications, stability of high-performance is crucial for AFE capacitors. The electric-driven phase transition engineering should provide a simple and universal route for the dramatic enhancement of capacitance and its stabilization, thus could be a highly effective complementary tactic to the elaborate compositional tailoring processes. Because the AFE-FE transition belongs to the ferroic transition, it is promising to witness similar strategy employed in stress-induced martensite phase transition or magnetic-induced antiferromagnetic-ferromagnetic phase transition for the substantial improvement of certain performances.

Methods

Sample preparation

Utilizing solid-state sintering method, the ceramic samples were synthesized by using the weighed raw oxide powders (purity of at least 99.0% of Pb_3O_4 , ZrO_2 , TiO_2 , La_2O_3 and SnO_2) and 0.5 wt% excess Pb_3O_4 . The mixed powders were dried, pressed and then calcined at 900 °C for 2 h. The calcined material was performed with ball-milling again for 24 h, drying, mixing with 6 wt% PVA as binding, and taking shape as pellets by vulcanization machine in a 13 mm diameter die at 150 MPa. After burning off PVA at 800 °C for 2 h, the pellets were sintered at 1300 °C for 2 h.

Using the same powders, MTI MSK-AFA-II tape caster and DEK 247 screen printer were used to fabricate MLCCs with 70Ag/30Pd electrode. The stacked layers were hot-pressed at 80 °C for 20 minutes and then sintered at 1100 °C for 2 h.

Electrical measurements

Ceramic samples having an electrode size of 8.8 mm diameter and an approximate thickness of 0.38 mm were used for the capacitance measurements. Ceramic samples for the other electrical measurements were polished to the thickness of 0.10–0.15 mm and the silver thin film was sputtered with the diameter of 0.75 mm as electrode. The P-E hysteresis loops were measured with aix ACCT TF 2000 analyzer ferroelectric measurement system (aix ACCT Co., Aachen, Germany) at 10 Hz. Dielectric properties of ceramics and MLCCs were measured with broad frequency dielectric spectrometer (Novocontrol GmbH, Concept 80).

Transmission electron microscope characteristics

The ceramics were prepared as a TEM thin-foil sample using traditional steps, including cutting, grinding, polishing, ion-milling and coating thin carbon films. A JEM-2100F microscope was used to acquire dark-field images and selected area electron diffraction patterns. In-situ biasing transmission electron microscopic experiments were performed on the JEOL JEM-2100F microscope. A home-made double-tilting TEM electrical holder was used for applying an electric field of up to E_{AF} in ramping mode, where E_{AF} is judged by the disappearance

of satellite spots and/or domain structures. The traditional TEM thin-foil sample was plated with two half-moon shaped Au electrodes and then wired with TEM electrical holder, and the corresponding schematic diagram of in-situ TEM thin-foil sample is showed in Fig. S15. The atomic-scale high-angle annular dark-field (HAADF) imaging was carried out on a Cs-corrected Hitachi HF5000 microscope with ultra-high resolution (UHR) mode and a convergence/collection semi-angle of 20mrad/60–320mrad. The atomic column positions at picometer-precision fitting was operated by MATLAB code^{43,44}.

Data availability

The data that support the findings of this study are available on request from the corresponding authors.

References

- Zhang, M. et al. Ultrahigh energy storage in high-entropy ceramic capacitors with polymorphic relaxor phase. *Science* **384**, 185–189 (2024).
- Li, J. et al. Grain-orientation-engineered multilayer ceramic capacitors for energy storage applications. *Nat. Mater.* **19**, 999–1005 (2020).
- Li, J. L. et al. Multilayer lead-free ceramic capacitors with ultrahigh energy density and efficiency. *Adv. Mater.* **30**, 1802155 (2018).
- Zhao, P. et al. Ultra-high energy storage performance in lead-free multilayer ceramic capacitors via a multiscale optimization strategy. *Energy Environ. Sci.* **13**, 4882–4890 (2020).
- Ma, Z. et al. High-performance energy-storage ferroelectric multilayer ceramic capacitors via nano-micro engineering. *J. Mater. Chem. A* **11**, 7184–7192 (2023).
- Feng, M. J. et al. Recent advances in multilayer-structure dielectrics for energy storage application. *Adv. Sci.* **8**, 2102221 (2021).
- Ge, G. L. et al. Synergistic optimization of antiferroelectric ceramics with superior energy storage properties via phase structure engineering. *Energy Stor. Mater.* **35**, 114–121 (2021).
- Qi, T. et al. Advanced dielectrics for capacitors. *IEEJ Trans. Fund. Mater.* **126**, 1153 (2006).
- Kwon, S. et al. Nonlinear dielectric ceramics and their applications to capacitors and tunable dielectrics. *IEEE Electr. Insul. Mag.* **27**, 43–55 (2011).
- Kim, I. et al. Characteristics of antiferroelectric PbZrO₃ Thin Films. *J. Korean Phys. Soc.* **33**, 180–183 (1998).
- Li, H. et al. Nonlinear capacitors for ESD protection. *IEEE Electro-magn. Compat. Mag.* **1**, 38–46 (2012).
- Pierre, T. et al. Theory of antiferroelectric phase transitions. *Phys. Rev. B* **94**, 014107 (2016).
- Jiang, R. J. et al. Atomic insight into the successive antiferroelectric-ferroelectric phase transition in antiferroelectric oxides. *Nano Lett.* **23**, 1522–1529 (2023).
- Zhang, J. et al. Plastic deformation in silicon nitride ceramics via bond switching at coherent interfaces. *Science* **378**, 371–376 (2022).
- Chen, H. et al. Unprecedented non-hysteretic superelasticity of [001]-oriented NiCoFeGa single crystals. *Nat. Mater.* **19**, 712–718 (2020).
- Chen, Y. et al. Phase engineering of nanomaterials. *Nat. Rev. Chem.* **4**, 243–256 (2020).
- Liu, X. et al. On-device phase engineering. *Nat. Mater.* **1**, 1476–1122 (2024).
- Qian, X. et al. High-entropy polymer produces a giant electrocaloric effect at low fields. *Nature* **600**, 664–669 (2021).
- Hao, X. et al. A comprehensive review on the progress of lead zirconate-based antiferroelectric materials. *Prog. Mater. Sci.* **63**, 1–57 (2014).
- Si, Y. et al. Antiferroelectric oxide thin-films: Fundamentals, properties, and applications. *Prog. Mater. Sci.* **142**, 101231 (2024).
- Wang, G. et al. Electroceramics for high-energy density capacitors: Current status and future perspectives. *Chem. Rev.* **121**, 6124–6172 (2021).
- Tan, X. et al. The antiferroelectric ↔ ferroelectric phase transition in lead-containing and lead-free perovskite ceramics. *J. Am. Ceram. Soc.* **94**, 4091–4107 (2011).
- Zhang, M. H. et al. Review on field-induced phase transitions in lead-free NaNbO₃-based antiferroelectric perovskite oxides for energy storage. *J. Materiomics* **9**, 1–18 (2023).
- Wei, X. K. et al. Progress on emerging ferroelectric materials for energy harvesting, storage and conversion. *Adv. Energy Mater.* **12**, 2201199 (2022).
- Qi, H. et al. Local structure engineered lead-free ferroic dielectrics for superior energy-storage capacitors: A review. *Energy Stor. Mater.* **45**, 541–567 (2022).
- Zhang, T. F. et al. Superior energy storage performance in antiferroelectric epitaxial thin films via structural heterogeneity and orientation control. *Adv. Funct. Mater.* **34**, 2311160 (2024).
- Liu, C. H. et al. Low voltage-driven high-performance thermal-switching in antiferroelectric PbZrO₃ thin films. *Science* **382**, 1265–1269 (2023).
- Zhao, H. et al. Excellent energy storage performance of ZnO doped (Pb,La)(Zr,Sn,Ti)O₃ based antiferroelectric ceramics at an ultra-low sintering temperature of 940°C. *Adv. Funct. Mater.* **34**, 2316674 (2024).
- Wang, H. S. et al. Ultrahigh energy-storage density in antiferroelectric ceramics with field-induced multiphase transitions. *Adv. Funct. Mater.* **29**, 1807321 (2019).
- Ge, G. L. et al. Optimizing the energy storage properties of antiferroelectric ceramics by modulating the phase structure via constructing a novel binary composite. *J. Mater. Chem. A* **9**, 11291 (2021).
- Liu, H. et al. Electric-field-induced structure and domain texture evolution in PbZrO₃-based antiferroelectric by in-situ high-energy synchrotron X-ray diffraction. *Acta Mater.* **184**, 41–49 (2020).
- Lu, T. et al. Critical role of the coupling between the octahedral rotation and A-site ionic displacements in PbZrO₃-based antiferroelectric materials investigated by in situ neutron diffraction. *Phys. Rev. B* **96**, 214108 (2017).
- Jin, L. et al. Decoding the fingerprint of ferroelectric loops: Comprehension of the material properties and structures. *J. Am. Ceram. Soc.* **97**, 1–27 (2014).
- Fu, Z. Q. et al. Unveiling the ferroelectric nature of PbZrO₃-based antiferroelectric materials. *Nat. Commun.* **11**, 3809 (2020).
- Zhang, L. et al. Chemically tunable textured interfacial defects in PbZrO₃-based antiferroelectric perovskite oxides. *Chem. Mater.* **33**, 6743–6751 (2021).
- Hu, T. F. et al. Hierarchical domain structures in (Pb, La)(Zr, Sn, Ti)O₃ antiferroelectric ceramics. *Ceram. Int.* **46**, 22575–22580 (2020).
- Randall, C. A. et al. Antiferroelectrics: History, fundamentals, crystal chemistry, crystal structures, size effects, and applications. *J. Am. Ceram. Soc.* **104**, 3775–3810 (2021).
- Sawaguchi, E. et al. Antiferroelectric structure of lead zirconate. *Phys. Rev.* **83**, 1078 (1951).
- Kittel, C. Theory of Antiferroelectric Crystals. *Phys. Rev.* **82**, 729–732 (1951).
- Ma, T. et al. Uncompensated polarization in incommensurate modulations of perovskite antiferroelectrics. *Phys. Rev. Lett.* **123**, 217602 (2019).
- Chen, L. et al. High-electromechanical performance for high-power piezoelectric applications: Fundamental, progress, and perspective. *Prog. Mater. Sci.* **127**, 100944 (2022).
- Lv, X. et al. Nano-domains in lead-free piezoceramics: a review. *J. Mater. Chem. A* **8**, 10026–10073 (2020).

43. Aert, S. V. et al. Advanced electron crystallography through model-based imaging. *IUCr. J.* **3**, 71–83 (2016).
44. De Backer, A. et al. StatSTEM: An efficient approach for accurate and precise model-based quantification of atomic resolution electron microscopy images. *Ultramicroscopy* **171**, 104–116 (2016).

Acknowledgements

This work is supported by the National Natural Science Foundation of China (52302136, U2230104, 52272130, 52002388 and U2002217), Young Elite Scientists Sponsorship Program by CAST (2022QNRC001), Shanghai Rising-Star Program (23QA1410800), China Postdoctoral Science Foundation (2023M743647), Zhejiang Province Postdoctoral Research Project Selected Funding (ZJ2023104), Shanghai Science and Technology Innovation Action Plan (21ZR1472400), and Shanghai technical platform for testing and characterization on inorganic materials (19DZ2290700).

Author contributions

T.H., Z.F., and X.C. conceived the experiments. L.L., C.X., Y.Z., F.C., and J.X. synthesized the samples and measured macroscopic properties. T.H. and X.L. performed the TEM experiments. T.H., Z.F., X.C., G.W., and F.X. analyzed the data, wrote, and edited the manuscript. All authors contributed to the discussion and manuscript preparation.

Competing interests

The authors declare no competing interests.

Additional information

Supplementary information The online version contains supplementary material available at <https://doi.org/10.1038/s41467-024-53661-z>.

Correspondence and requests for materials should be addressed to Zhengqian Fu, Xuefeng Chen, Genshui Wang or Fangfang Xu.

Peer review information *Nature Communications* thanks Rongli Gao and the other anonymous reviewer(s) for their contribution to the peer review of this work. A peer review file is available.

Reprints and permissions information is available at <http://www.nature.com/reprints>

Publisher's note Springer Nature remains neutral with regard to jurisdictional claims in published maps and institutional affiliations.

Open Access This article is licensed under a Creative Commons Attribution-NonCommercial-NoDerivatives 4.0 International License, which permits any non-commercial use, sharing, distribution and reproduction in any medium or format, as long as you give appropriate credit to the original author(s) and the source, provide a link to the Creative Commons licence, and indicate if you modified the licensed material. You do not have permission under this licence to share adapted material derived from this article or parts of it. The images or other third party material in this article are included in the article's Creative Commons licence, unless indicated otherwise in a credit line to the material. If material is not included in the article's Creative Commons licence and your intended use is not permitted by statutory regulation or exceeds the permitted use, you will need to obtain permission directly from the copyright holder. To view a copy of this licence, visit <http://creativecommons.org/licenses/by-nc-nd/4.0/>.

© The Author(s) 2024